J. Fluid Mech. (2006), *vol.* 556, *pp.* 309–327. © 2006 Cambridge University Press
doi:10.1017/S0022112006009487 Printed in the United Kingdom

Combined polymer and microbubble drag reduction on a large flat plate

By STEVEN DEUTSCH, ARNOLD A. FONTAINE, MICHAEL J. MOENY AND HOWARD L. PETRIE

The Applied Research Laboratory, The Pennsylvania State University, University Park, PA 16804, USA

(Received 1 December 2004 and in revised form 28 November 2005)

Drag-reduction experiments with combined injection of high-molecular-weight long-chained polymers and microbubbles were conducted on a 3.1 m long flat plate model in the 1.22 m diameter water tunnel at the Applied Research Laboratory of the Pennsylvania State University. Combined gas injection upstream of polymer injection produced, over a wide range of test conditions, higher levels of drag reduction than those obtained from the independent injection of polymer or microbubbles alone. These increased levels of drag reduction with combined injection were often greater than the product of the drag reductions obtained by the independent constituents, defined as synergy. We speculate that the synergy is a result of the gas-layer-induced extension of the polymer-alone initial diffusion zone in combination with the increased drag reduction by microbubbles. This increased length of the initial zone layer, consistent with high drag reduction, can significantly increase the persistence of the drag reduction and may improve the outlook for practical application.

1. Introduction

The introduction of solutions of long-chained polymer molecules or of gas to form microbubbles into a turbulent boundary layer has long been known to reduce skin-friction drag. The mechanisms responsible for drag reduction by either of these methods are not yet fully understood. However, Tiederman, Luchik & Bogard (1985) and Smith & Tiederman (1990) showed that polymer molecules are effective only when located in the buffer region of the turbulent boundary layer and Pal, Deutsch & Merkle (1989) reached essentially the same conclusion regarding microbubbles.

The first detailed studies of slot-injected polymer drag reduction were those of Wu & Tulin (1972), who considered drag reduction as a function of polymer concentration and injection flow rate. Poreh & Hsu (1972) considered the diffusion aspects of the polymer injection problem. Their work was modelled after the classical experimental results of Poreh & Cermak (1964) for the diffusion of a passive contaminant from a line source. Poreh & Cermak (1964) characterized the injectant diffusion process by identifying, as a function of diffusion-layer thickness to boundary-layer thickness, four diffusion zones. In the initial diffusion zone, the contaminant resides in a thin layer at the wall of the order of the viscous sublayer to a small fraction, 1/10, of the boundary-layer thickness. Poreh & Hsu (1972) determined that the diffusion zone results of Poreh & Cermak (1964) were qualitatively useful in characterizing the polymer diffusion process. Whereas for a passive contaminant the initial diffusion

https://doi.org/10.1017/S0022112006009487 Published online by Cambridge University Press

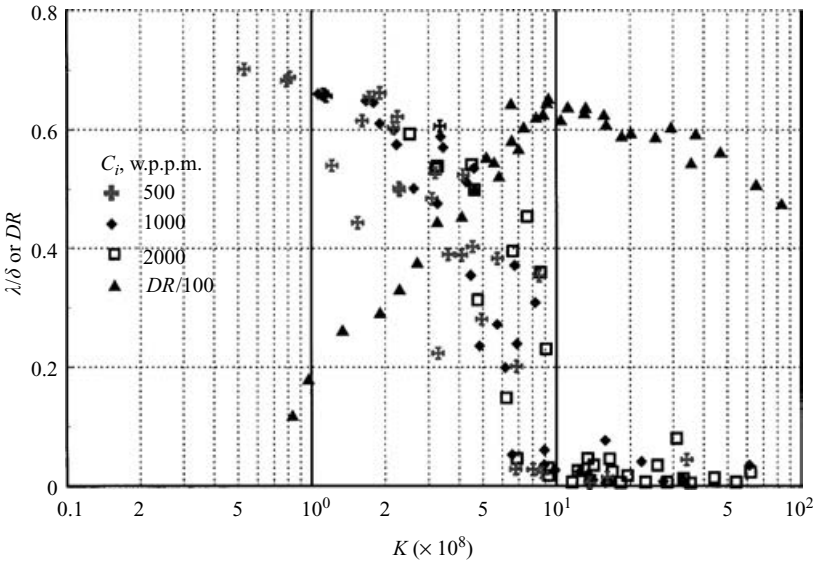


FIGURE 1. Diffusion-layer development versus K factor compared to local drag reduction with PEO WSR 301 injection (Petrie *et al.* 1996). ▲, fractional drag reduction.

zone is of the order of millimetres, Poreh & Hsu (1972) estimated that the initial diffusion zone for polymer could be up to 3 orders of magnitude larger.

Fontaine, Petrie & Brungart (1992) used laser-Doppler velocimetry to analyse slot-injected polymer in an external boundary layer. They showed that the primary effect of injected polymer is the suppression of vertical velocity fluctuations and Reynolds shear stress in the near-wall region. The suppression of turbulent transport properties results in a reduction in the diffusion of the polymer away from the wall. This result is significant as Vdovin & Smol'yakov (1978, 1981) and Petrie, Fontaine & Brungart (1996*a*) and Petrie *et al.* (2005) have identified the initial diffusion zone as the region of high drag reduction. We reproduce the results of Petrie *et al.* (1996*a*) as figure 1. Here, concentration has been measured by doping the polymer with fluorescent dye and using an optical technique described by Brungart *et al.* (1991). This optical technique provides a local estimate of the concentration profile as a function of the distance from the wall, while drag reduction was measured using floating-element force balances that averaged the measured skin friction over a finite span of the plate. The increased scatter in the diffusion-layer thickness profiles (given by λ/δ, where λ is the 50 % diffusion-layer thickness and δ is the 99 % boundary-layer thickness) compared to the drag reduction data is, in part, a result of minor and expected spanwise variability in the polymer concentration profile exiting the slot. Figure 1 has been reproduced here merely to illustrate that high drag reduction correlates with a thin initial-diffusion-zone polymer layer (low λ/δ) where wall concentrations are larger. The trend is clear.

We define drag reduction (DR) as the ratio of measured skin friction under injection conditions to measured skin friction without injection, subtracted from one. In figure 1, the right-hand side of this equation was multiplied by a factor of 100, so the resulting value would range between 0 and 100 %,

$$DR = 1 - \left(\frac{F_{inj}/A}{F_o/A}\right). \tag{1}$$

https://doi.org/10.1017/S0022112006009487 Published online by Cambridge University Press

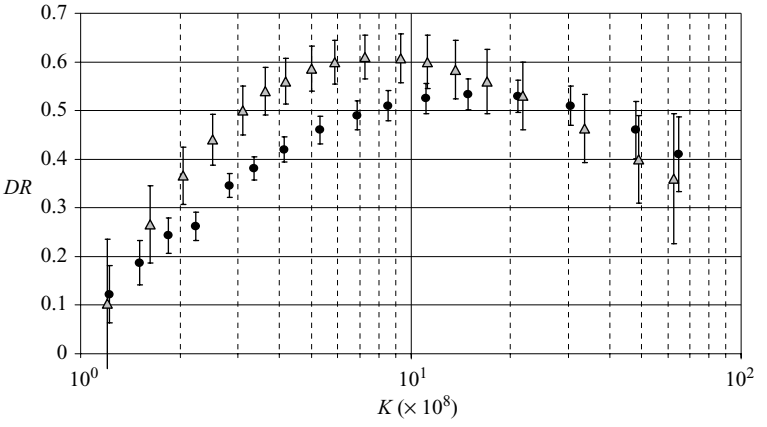


FIGURE 2. Comparison of drag reduction versus K factor for (●) PEO WSR301 and (△) UCARFLOC 309.

The parameter $K = Q_p C_i/\rho U_e X_S$ (or $Q_p C_i/\mu(1/Re_x)$), used in figure 1, was first developed by Vdovin & Smol'yakov (1978, 1981). Here, Q_p is the polymer flow rate per unit span of the injection slot, C_i the polymer injection concentration in units of density, U_e the mean velocity and X_S the distance from the slot. The numerator in the K-factor scaling represents the polymer-solution expenditure rate, while the denominator is related to the diffusion process.

The initial zone, where $\lambda/\delta < 0.1$, is apparent for $K \times 10^8 \geqslant \sim 7$ to 10 in figure 1. For $K \times 10^8 > 7$, the drag reductions are large, the diffusion layer is thin, and the polymer concentration profiles have a form characteristic of the initial diffusion zone (Petrie *et al.* 1996*a*, *b*). Relatively farther downstream, with lower K, both the drag reduction and the near-wall polymer concentration drop off rapidly. This rapid change in the slope of the drag reduction versus K curve, near $K \times 10^8 = 10$, denotes a change from initial-zone to transition-zone behaviour in the diffusion process (Poreh & Hsu 1972; Vdovin & Smol'yakov 1981).

More effective drag-reducing polymers (higher molecular weight) extend the initial diffusion zone farther downstream of the slot or to lower K (Vdovin & Smol'yakov 1981). Figure 2 compares drag reductions with WSR301 and UCARFLOC 309 solution injection. Both polymers are polyethylene oxide (PEO) blends manufactured by Dow Chemical. The mean molecular weight of UCARFLOC 309 is approximately 8×10^6, based on the manufacturers estimate, compared to 4×10^6 for WSR301. The approximate end of the initial diffusion zone, where the drag reduction begins to decrease rapidly with decreasing K, is roughly at $K \times 10^8 \sim 6$ for UCARFLOC 309 drag reduction and at $K \times 10^8 \sim 10$ for WSR301. The two data sets represent curve fits to many repeat runs of each polymer condition covering a range of injection rates, free-stream velocities and balance locations downstream of the injector. The error bars reflect the 95 % confidence interval of the variability in the data about the curve fit at each K. Petrie *et al.* (2005) have shown a similar trend in a shift in the drag reduction versus K factor scaling with a comparison of WSR301 and N60K (Dow Chemical). The manufacturers' estimate of the molecular weight of N60K is 2×10^6. The location where the N60K drag reduction begins to decrease rapidly with decreasing K is roughly $K \times 10^8 = 20$, or approximately a factor of two increase in K relative to the WSR301 value (Petrie *et al.* 2005).

https://doi.org/10.1017/S0022112006009487 Published online by Cambridge University Press

High levels of microbubble drag reduction have been achieved by the direct injection of gas through slots or porous materials (Migirenko & Evseev 1974; Bogdevich & Evseev 1976; Bogdevich & Malyuga 1976; Merkle & Deutsch 1989). The primary parameter is the actual gas flow rate (Q_g) referenced to the ambient conditions of temperature and pressure at the injector (Madavan, Deutsch & Merkle 1985; Fontaine & Deutsch 1992). Microbubble drag reduction does not appear to be strongly influenced by gas type (Fontaine & Deutsch 1992) or method of injection (Merkle & Deutsch 1989). Pal *et al.* (1989) found that the frequency spectra and higher-order moments of the wall shear stress fluctuation statistics in microbubble drag reduction were remarkably similar to that observed with polymer injection. Merkle & Deutsch (1990) provide a comprehensive review of early attempts at skin-friction reduction by microbubble injection.

Practical application of either technique will ultimately result in a need to reduce the consumption rate of the injectant and this has provided an impetus to investigate combinations of the two. Malyuga, Mikuta & Nenashev (1989) measured the skin-friction reduction produced by aerating PEO WSR301, to produce a two-phase polymer gas mixture (froth), prior to slot-injection. The authors reported lower levels of skin friction when injecting aerated polymer than with comparable injection rates of polymer alone. Additionally, they note that the level of drag reduction achieved by a given aerated polymer solution was inversely related to the level of drag reduction achieved by that polymer solution without aeration.

Fontaine *et al.* (1999) reported the effect of microbubble injection into a dilute homogeneous polymer 'ocean' on an axisymmetric body. Measured drag-reduction levels for gas injection into a polymer ocean were higher than levels obtained for either polymer ocean or microbubble injection alone. The increase in drag reduction was found to follow a multiplicative relationship (equation (2)), with no evidence of cooperative action.

$$\left(\frac{C_f}{C_{f0}}\right)_{Absolute} = \left(\frac{C_f}{C_{f0}}\right)_{Polymer\ alone} \left(\frac{C_f}{C_{f0}}\right)_{Microbubble\ alone} \tag{2}$$

The ratio of C_f/C_{f0} represents the drag reduced estimate of the skin-friction coefficient normalized by the baseline value of the skin-friction coefficient without drag reduction. These results suggest that the drag reduction with homogeneous polymer ocean acts independently of the mechanism induced by microbubble injection. Similar results are obtained for polymer injected into a homogeneous polymer solution (Petrie *et al.* 2003).

Philips, Castano & Stace (1998) measured drag reduction with combined microbubble and PEO WSR301 injection in sea-water on a 2.73 m long $\times$ 0.305 m span flat plate. Gas injection upstream of the polymer injection consistently produced more drag reduction than expected based on the individual injections. This effect was confined to levels of microbubble injection which produced less than 30 % drag reduction. The highest levels of this effect were achieved for low microbubble injection rates over nearly all polymer injection rates. The authors defined synergy as a reduction in skin-friction drag during combined injection greater than the sum of each drag reduction observed during individual injection, thus, they defined synergy as an additive interaction. Air injection downstream of the polymer injection produced lower levels of drag reduction than the sum of the individual reductions.

In the current study, synergy from combined injection is defined as the difference between the product of the skin-friction coefficient ratio with each material injected

https://doi.org/10.1017/S0022112006009487 Published online by Cambridge University Press

separately and the skin friction coefficient ratio with combined injection, C_{fGP}/C_{f0}:

$$SYNERGY = \left(\frac{C_{fGas}}{C_{f0}}\frac{C_{fPolymer}}{C_{f0}}\right) - \frac{C_{fGP}}{C_{f0}}. \tag{3}$$

Since Fontaine *et al.* (1999) has shown that the drag reduction due to the injection of micro-bubbles into a polymer ocean is multiplicative, this definition is self-consistent.

The influence of combined injection on the persistence of drag reduction is examined in this study. The objectives were to determine whether there is a synergistic benefit with combined gas and polymer injection, and to determine the conditions for which it occurs. Another goal was to determine the effect of combined injection on the persistence of the drag reduction. To best study persistence, the inverse of the K factor was used as the independent parameter. This removes a singularity at the injector and is, perhaps, more intuitive. Vdovin & Smol'yakov (1978, 1981) introduced a diffusion length L based on the decay of the polymer wall concentration and plotted drag-reduction data versus X_S/L. In the present study, polymer and micro-bubble decay lengths were defined as $L_p = Q_p C_i/\rho U_e$ and $L_m = Q_g/U$.

2. Experimental approach

Experiments were conducted on a flat-plate model installed in a water tunnel at the Applied Research Laboratory at the Pennsylvania State University. The tunnel test section has a diameter of 1.22 m and a length of 4.27 m. The 0.07 m thick plate is 3.1 m long and 1.22 m in span and was mounted on the horizontal centreplane of the tunnel. The working surface of the plate was oriented up, opposite gravity, such that buoyancy was directed away from the surface. The leading edge consists of a 6:1 elliptical nose section. A near zero pressure gradient is maintained along the plate using an adjustable wedge-shaped tail section at the trailing edge. The tail section was adjusted to provide a slight negative angle of attack on the nose, fixing the dividing streamline. The boundary layer developed naturally from a relatively stationary virtual origin near the leading edge of the plate.

Petrie *et al.* (1990) performed axial free-stream laser-Doppler velocimetry surveys along the plate and showed the free-stream velocity varied by less then 0.5 % along the plate over the central 50 % span of the plate. This measured velocity variation correlates to a C_p variation of less than ± 0.01. Flow over the central 50 % span of the plate is turbulent, two-dimensional and fully developed over the working length of the plate. Additional wall normal laser-Doppler velocimetry surveys were taken at $z = 0$ m (on centreline, CL), 0.305 m and 0.457 m at approximately 0.3 m downstream from the gas slot, X_S, and at $z = 0$ m (on CL), 0.127 m and 0.305 m at approximately 1.6 m downstream of the gas slot. The survey at $X_S = 0.3$ m indicated that corner flow effects consistent with 10° wedge growth were present at the $z = 0.457$ m location, near the sidewalls. No corner flow effects were apparent in any of the surveys taken at $X_S = 1.6$ m. One explanation for this is that flow is observed to move through the plate side regions. This flow is the result of a slight pressure differential between the upper and lower surfaces of the plate, coupled with the small sidewall gaps, and may inhibit the growth of the corner flow disturbance.

Measured boundary-layer parameters are given in table 1. Momentum thickness Reynolds numbers are as high as 39 000. In this table, X_o is the streamwise distance along the plate measured from the estimated turbulent-boundary-layer virtual origin, as determined by the functional dependence of δ, δ^* and θ on X. The friction velocity u^* is determined by a Clauser plot analysis of laser-Doppler velocimetry measured

https://doi.org/10.1017/S0022112006009487 Published online by Cambridge University Press

X_o (m)	U_e (m s^{-1})	R_{exo} ($\times 10^7$)	u^* (m s^{-1})	TBL thickness δ (mm)	Displacement thickness δ^* (mm)	Momentum thickness θ (mm)	$R_{e\theta}$ ($\times 10^3$)
0.694	9.37	0.651	0.336	8.8	1.4	1.0	13.31
0.959	9.4	1.97	0.328	13.4	1.9	1.4	13.54
1.45	9.24	0.899	0.326	20.2	2.6	2.0	18.3
	13.6	1.34	0.47	18.1	2.3	1.8	24.3
1.76	9.31	1.65	0.317	22.1	3.1	2.3	21.7
	13.41	2.35	0.45	20.7	2.5	1.9	26.0
2.1	8.92	1.87	0.302	26.6	3.6	2.7	24.3
	13.41	2.88	0.451	25.7	3.3	2.6	35.1
2.43	13.8	3.35	0.456	28.2	3.6	2.8	39.0

TABLE 1. Large flat-plate boundary-layer parameters.

velocity profiles in the log region of the turbulent boundary layer, and by a least-squares error fit of the boundary-layer data to the law of the wall plus Coles wake function (see Deutsch & Zierke 1986).

Combined polymer and microbubble injection was accomplished through a dual-injector assembly composed of two spanwise oriented slots that spanned the central 59.7 cm of the test plate. The injection-slot design has an effective throat width of $\sim$1.6 mm and is described in Petrie *et al.* (2003, 2004). The upstream injection slot is $\sim$0.6 m from the leading edge of the plate, while the second slot is 39 mm further downstream. This separation is approximately four boundary-layer thicknesses at 10.7 m s^{-1}. For this investigation, the upstream slot was used for microbubble injection and the downstream slot for polymer injection.

The plenum of the gas slot contained a two-layer baffle constructed from a 0.8 mm diameter perforated brass sheet topped by a coarse-grade non-metallic fibre pad to provide added pressure drop and increase spanwise uniformity. The plenum of the polymer slot contained a four-layer perforated brass baffle. Visual inspection of the bubble cloud and of an injected polymer and dye solution served to qualify the presence of both spanwise uniformity of the injectants and complete spanwise coverage at the downstream measurement location.

The upstream slot assembly is fed from a bank of three high-pressure dry-air cylinders. A Grove model 202G dome-loader regulated inlet line pressure. Gas flow rate was adjusted and controlled using a Kates constant-flow control valve. The gas mass flow rate was measured with a Sierra Model 530 mass-flow meter. The meter is routinely factory calibrated and has a reported accuracy of ± 0.5 % of full scale. Gas temperature is monitored just upstream of the tunnel penetration by a StoLab Electronic Thermometer (Model 911L). This information, along with tunnel static pressure (measured by 344 750 Pa Foxboro model 1800), is used to convert the mass flow to a volume flow rate at injector conditions.

The downstream slot assembly is fed from a 300 l pressurized tank. The pressure side of the tank uses a regulated high-pressure air supply: the constant pressure provides a nearly constant flow rate during injection. Polymer flow rate, controlled using a ball valve, was measured with a Bailey–Fisher and Porter Series 10D1475Y MINI_MAG Magnetic flowmeter. The magnetic flowmeter calibration is insensitive to viscoelastic fluid characteristics, and has a rated uncertainty of less than 0.5 % of the reading.

https://doi.org/10.1017/S0022112006009487 Published online by Cambridge University Press

Skin friction is measured by six identical floating-element drag balances installed in three modules flush-mounted with the upper surface of the flat plate. The distances from the plate leading edge to the leading edge of each balance were: $X_{LE} = 0.703$, 0.873, 1.094, 1.546, 1.936, 2.495 m. Each drag balance consists of a 127 mm wide $\times$ 38 mm long floating shear plate mounted to a strain gauged shear flexure which is in turn rigidly mounted to the drag balance module assembly installed in the flat plate. Drag balances were calibrated with weights prior to installation and were linear with a regression coefficient of $R^2 > 0.999$. Gaps between the floating shear plates and the surrounding plate were maintained at 25 to 125 μm, where the majority of the gaps were less than 75 μm. Each shear plate was flush mounted with the surrounding surface to within 25 μm (at most 12 wall units) above or 50 μm below the surrounding plate as confirmed by dial depth gages.

Each balance assembly is mounted in a sealed cavity within the surrounding test plate. This cavity is flooded with water during installation of the balance assemblies to minimize the potential for trapped air below the balance shear plate. Care is taken to ensure that water is uniformly forced out of the gaps between the shear plates and the surrounding test surface during final installation. The good day-to-day repeatability of the drag-reduction data with gas injection alone would also argue against this being a common occurrence.

At the start of each day, force cell data were collected as the tunnel was stepped through the full range of velocities. This *in situ* calibration, along with non-injection data points taken frequently each day enabled the continual monitoring of the state of the force cells. This procedure allowed us to monitor polymer build up in the tunnel during the injection runs. Background polymer concentrations were deemed too high when either the background concentration approached one weight part per million (w.p.p.m.) or the baseline drag measurements exhibited greater than 5 % drag reduction. Once either of these conditions was reached, the tunnel was drained and refilled with fresh water, or the tunnel was operated at 16 m s^{-1} for an extended period of time (until drag balance measurements returned to normal) to degrade the background polymer.

Solutions of PEO UCARFLOC 309, with a mean molecular weight of about eight million, were hand-mixed in 100 l vats, as described by Petrie *et al.* (2003). Chlorine is known to negatively affect PEO solutions (Petrie *et al.* 2003). Therefore, both the mix water and the water tunnel volume were dechlorinated with sodium thiosulfate. The polymer mix was allowed to stand for several hours to hydrate. To avoid degradation of the solution, a peristaltic pump was used to transfer the polymer from the mixing vat to the injection tank.

Data were taken at free-stream velocities of 10.7, 13.7 and 16 m s^{-1} which result in Reynolds numbers of approximately 6.6 to 33.4 million, based on streamwise distance from the turbulent-boundary-layer virtual origin (64 mm upstream of the plate leading edge) to the leading edge of the drag balance shear plates. For a given combination of injection conditions, a test run was initiated by first starting the polymer injection and measuring the polymer only drag force. The gas injection was then initiated and combined injection drag was measured. Finally, the polymer injection was terminated and the gas only drag was measured. At each step, the tunnel was allowed to stabilize before data acquisition. Repeat test runs were conducted in a random order for several dual injection test conditions (U_e, Q_p and Q_g conditions) with 1000 w.p.p.m. UCARFLOC 309.

Air-injection volumetric flow rates per unit span of the injector were $Q_g = 0.0059$, 0.012 and 0.0218 m^2 s^{-1} (0.0035, 0.0073 and 0.013 m^3 s^{-1} measured flow rates). Each

https://doi.org/10.1017/S0022112006009487 Published online by Cambridge University Press

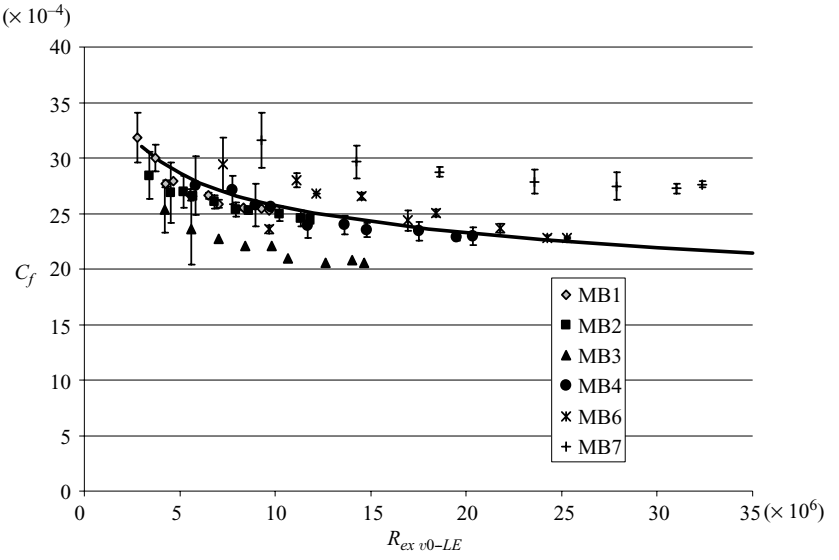


FIGURE 3. Measured skin friction versus Reynolds number with no injection. The solid line is the plot of C_f from equation (2), (White 1974).

successive injection rate is roughly twice the preceding rate. The three air-flow rates are referred to as low (L), medium (M) and high (H), respectively, in the figures. Polymer injection rates were 5 and 10 Q_s, where Q_s is the volume flow rate per unit span through the viscous sublayer defined as $0 < y^+ \leqslant 11.6$. A linear sublayer velocity profile yields a Q_s that is independent of velocity, $Q_s = 67.3\,\upsilon$ where υ is the fluid kinematic viscosity. To avoid cavitation at the higher velocities, tunnel static pressure was maintained at 2.41 kPa. Data acquisition is accomplished with a PC controlled IOTECH Model 516 Wave book and Model WBK16 Strain Gauge Module using DASYLab data acquisition software.

3. Results and discussion

The comparison of measured and empirical forces for the six drag balances without injection is shown in figure 3 plotted against Reynolds number. Each balance is represented by a unique symbol, and is shown with estimated error bars. Note that the uncertainty increases with decreasing Re_x (or force), as expected. Balance 5 failed early in the test and no data are presented for it. The solid line in figure 3 is the empirical skin friction calculated from equation (4), (White 1974),

$$C_f = 0.455/\ln^2(0.06Re_{vo-LE}), \tag{4}$$

which is said to be accurate to $\pm 2\,\%$ over the entire turbulent range.

The output from the force cells in positions 3 and 7 were low and high, respectively, when compared to theory. Throughout the experiment, the data for these two cells were consistent. The primary form for drag data presented in this paper is that of drag reduction, or $1 - F_{inj}/F_0$, where F_{inj} is the measured force during injection and F_0 is the baseline force measured without injection. Extending equation (1) with the C_f ratio, it is seen that as C_f is proportional to the drag force over the shear plate

https://doi.org/10.1017/S0022112006009487 Published online by Cambridge University Press

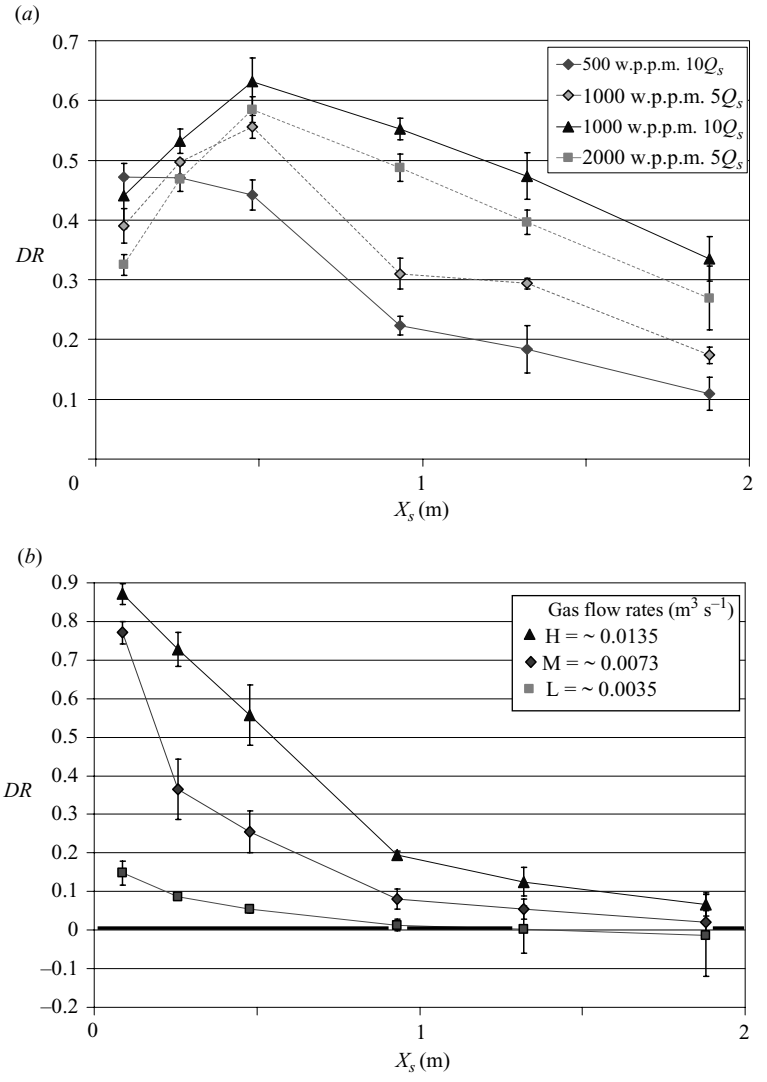


FIGURE 4. Comparison of drag reduction by polymer and microbubble injection at 16 m s^{-1}. (*a*) UCARFLOC 309 injected at various injection conditions. (*b*) Microbubble injection at three gas rates.

surface area, $C_f \propto F/A$, drag reduction is given by

$$DR = 1 - \frac{C_{f_{inj}}}{C_{f_0}} = 1 - \left(\frac{F_{inj}/A}{F_0/A}\right). \tag{5}$$

Since output of the force cells at positions 3 and 7 did not drift over time, a correction for the bias error to the data was unnecessary.

Typical single-injection drag-reduction results taken at a free-stream velocity of 16 m s^{-1} are shown in figures 4(*a*) and 4(*b*) for polymer and for microbubble injection. These figures illustrate the similarities and differences between the drag-reduction techniques with distance from the slot. Repeatability of the injection tests is indicated by the error bars to 95 % confidence levels. Figure 4(*a*) shows drag reduction as a

https://doi.org/10.1017/S0022112006009487 Published online by Cambridge University Press

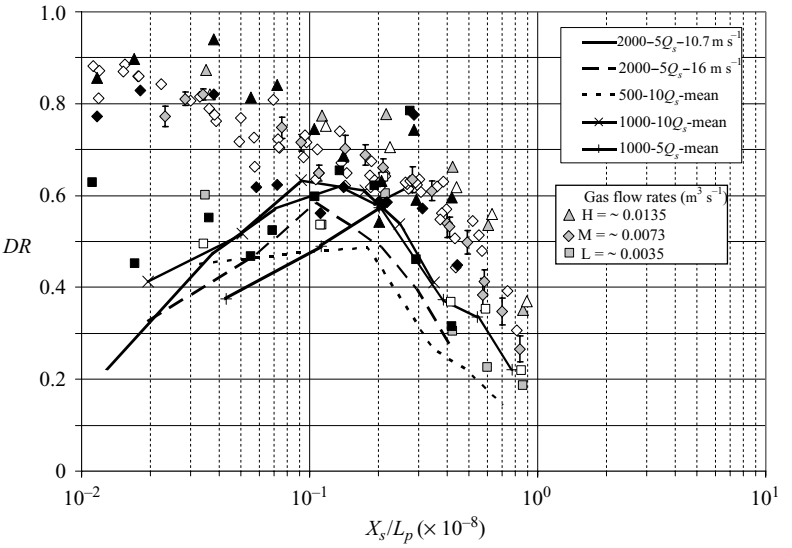


FIGURE 5. Drag reduction versus X_s/L_p for UCARFLOC 309 and combined injection. Grey symbols, 500 w.p.p.m.; open symbols, 1000 w.p.p.m; solid symbols, 2000 w.p.p.m.

function of streamwise distance for polymer injection of 500, 1000 and 2000 w.p.p.m. PEO UCARFLOC 309 at 5 and 10 Q_s. A downstream displaced peak in the drag-reduction curves is observed for the 1000 and 2000 w.p.p.m. data, while the 500 w.p.p.m. data peaks at the first measurement location. We suspect that the lower levels of drag reduction close to the slot for the higher-concentration cases may be a result of increased near-wall viscosity of the polymer solution ($\tau_w = \mu(\mathrm{d}U/\mathrm{d}y)$), see Petrie *et al.* 2003). Substantial drag reduction is still observed at the most downstream measurement location for the higher polymer consumption rates (Q_pC_i).

Microbubble drag reduction exhibits a different development process from that observed with polymer injection. Local drag-reduction levels from microbubble injection are highest at the most upstream balance and decrease steadily with increasing X_S, as shown in figure 4(*b*). In addition, drag reduction by microbubble injection near the slot increases with increasing injection rate, whereas increased polymer concentration can decrease the drag reduction near the slot. The microbubble drag reduction is less than 10 %, in all cases, at the position of the last balance.

3.1. *Combined injection*

Figure 5 presents drag-reduction results for single injection of PEO UCARFLOC 309 and combined injection of PEO UCARFLOC 309 with gas versus X_S/L_p where $L_p = Q_pC_i/\rho U_e$. Symbols represent combined injection and the lines indicate polymer injection. The plotted data cover a range of velocities from 10.7 to 16 m s^{-1} with Q_p of 5 and 10 Q_S and X_S up to 1.9 m. The most striking result on figure 5 is that the combined-injection drag reductions are consistently large near the injection slot, $X_S/L_p \times 10^{-8} < 0.1$, where drag reductions tend to be low with polymer injection alone. The error bars represent the 95 % uncertainty in the drag-reduction value determined through an uncertainty propagation analysis, following Coleman & Steele (1999), of the balance force uncertainties into the equation for drag reduction. The spread in the data for the initial diffusion zone region ($X_S/L_P \times 10^{-8} < 0.1$)

https://doi.org/10.1017/S0022112006009487 Published online by Cambridge University Press

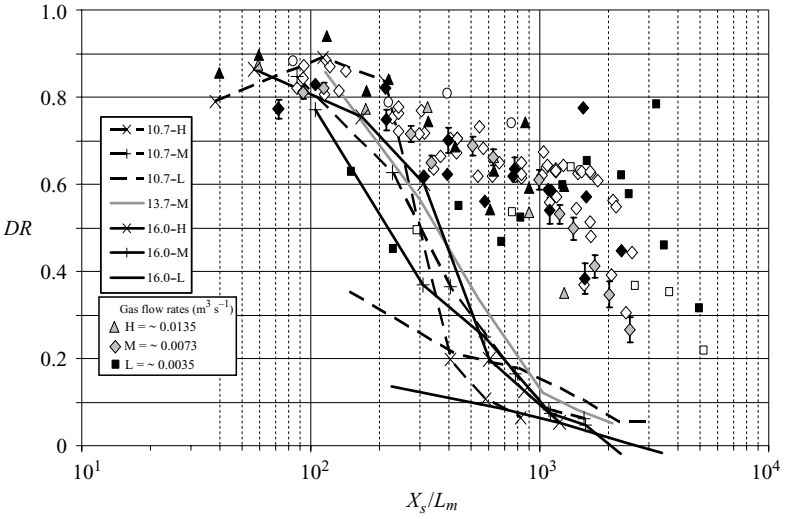


FIGURE 6. Drag reduction versus X_s/L_m for gas and combined injection. Grey symbols, 500 w.p.p.m.; open symbols, 1000 w.p.p.m; solid symbols, 2000 w.p.p.m.

is most probably variability due to increased polymer dynamic viscosity effects on the measured drag reduction (Petrie *et al.* 2003).

The bulk of the combined injection data is elevated relative to the polymer-only lines, indicating that a higher level of drag reduction is achieved for a given X_S/L_p. The data at the lowest X_S/L_p are typically data taken at low speeds or close to the injector. The data show that combined injection effectively eliminates the low polymer drag-reduction penalty close to the injection slot. The shift to higher X_S/L_p of the location where the magnitude of the negative slope of the drag reduction versus X_S/L_p relationship increases, at $0.3 \leqslant X_S/L_p \times 10^{-8} \leqslant 0.5$ on figure 5, is felt to be indicative of an extension of the initial diffusion zone with combined injection. This implies that gas injection can increase the length of the initial diffusion zone for a given set of velocity and polymer injection conditions.

Figure 6 presents the gas and combined injection data against X_S/L_m where $L_m = Q_g/U$. The symbols are combined injection data, the lines are gas injection alone. This plot shows that the drag-reduction levels for the combined injection approximately match those of the micro-bubble injection alone for $X_S/L_m < 200$. These locations are close to the injection slot. The most dramatic feature, however, is the much slower decrease in drag reduction with increasing X_S/L_m when compared with microbubble injection alone.

Figure 7 illustrates the range of variability observed in the synergy values, defined by equation (3), for the repeat runs of dual injection with 1000 w.p.p.m. UCARFLOC 309. The data points in figure 7 are the mean values of the repeat synergy results at each X_S/L_p. The error bars represent the maximum and minimum spread in the repeat data about the mean value.

Figure 8 plots synergy as a function of X_S/L_p for 500 w.p.p.m. polymer and all gas flow rates. The low gas-flow-rate case produces the lowest levels of synergy, generally less than 0.1. This low gas injection is also the only case which does not exhibit negative levels of synergy at the most upstream balance. Negative synergy simply means that the drag-reduction value based on the independent multiplicative effect is greater than the measured combined injection value. The medium and high gas

https://doi.org/10.1017/S0022112006009487 Published online by Cambridge University Press

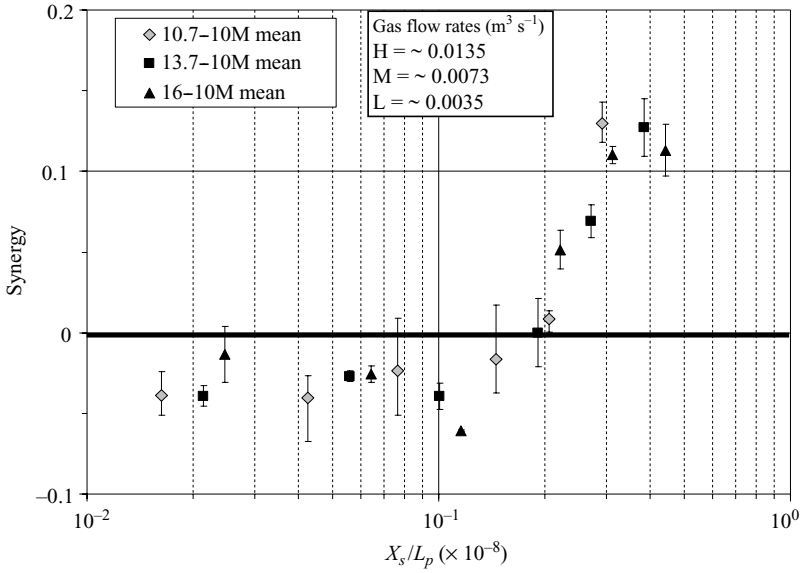


FIGURE 7. Summary of repeat test runs of synergy levels for air over 1000 p.p.m. UCARFLOC 309. Error bars represent the minimum and maximum spread in synergy data ensembles about the mean of the synergy repeat runs.

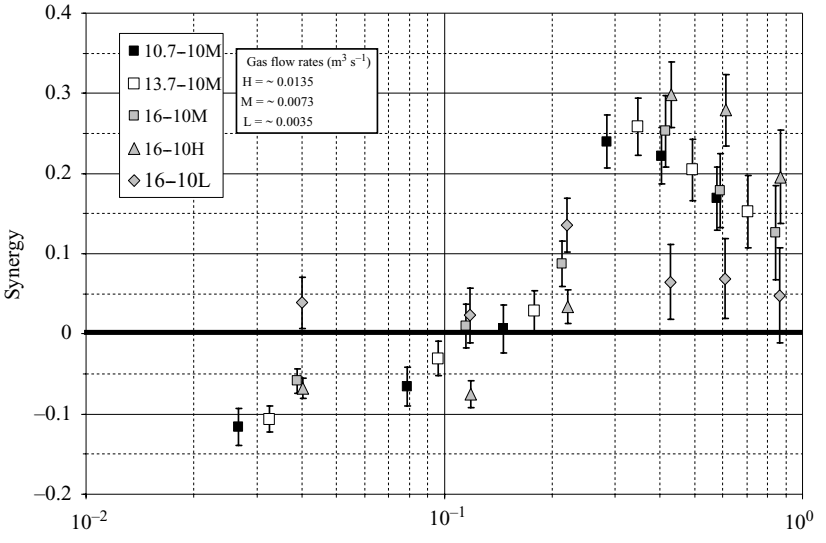


FIGURE 8. Synergy levels for air over 500 p.p.m. UCARFLOC 309.

injection rates produce the highest levels of synergy, peaking at about 0.25 to 0.30. The synergy lines for the combination of $10Q_S$ polymer injection with medium and high gas-flow rates peak at nearly a factor of 2 larger X_S/L_p than observed with the low gas injection cases. We believe this shift to higher X_S/L_p suggests the polymer diffusion away from the wall is slowed by the effect of the bubble injection and the polymer initial diffusion zone is lengthened.

https://doi.org/10.1017/S0022112006009487 Published online by Cambridge University Press

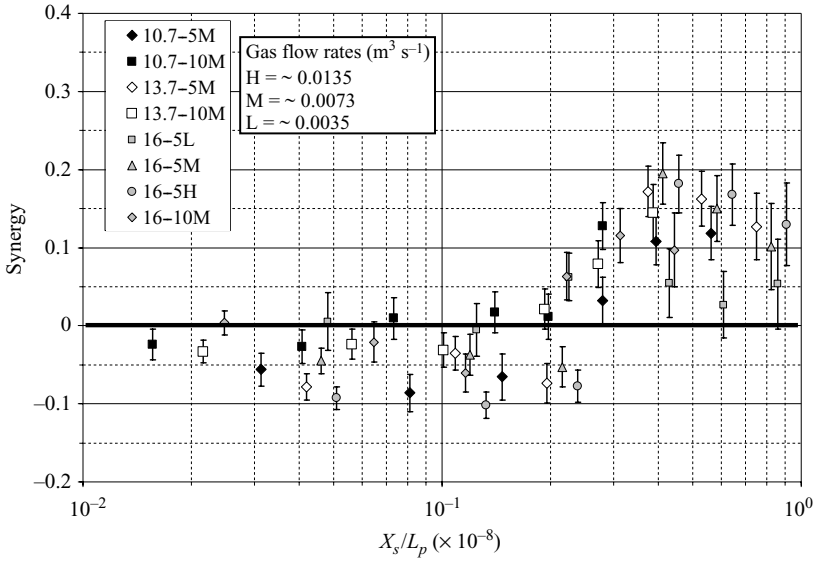


FIGURE 9. Synergy levels for air over 1000 p.p.m. UCARFLOC 309.

The negative synergy levels at $X_S/L_p \times 10^{-8} < 0.1$ in figure 8 may simply indicate that the benefit of reduced polymer diffusion by gas injection has little effect this near to the slot where much of the injected polymer is still close to the surface without bubble injection. The effect of a sustained reduction on the diffusion rate of polymer away from the surface should be seen farther downstream. The high skin-friction drag reduction from micro-bubbles alone may create a situation where the polymer can have little or no effect. The flow may be effectively saturated at these high drag reductions. Also, polymer drag reduction is dependent on the Weissenberg number, $We = T_p u^{*2}/\nu$ where T_p is the polymer relaxation time and u^* is the friction velocity (see Housiadas & Beris 2003). An 80 % reduction of the skin friction by bubbles corresponds to an 80 % reduction of the Weissenberg number that the polymer would experience initially after injection. Housiadas & Beris (2003) observe that, at sufficiently low *We*, drag reduction is sensitive to *We* and decreases with decreasing *We*. Also, as noted earlier, the high polymer viscosity near the slot may act to offset drag-reduction benefits obtained by the gas injection near the slot.

Figure 9 presents combined injection data for 1000 w.p.p.m. polymer in the same manner as figure 8. Note that all cases exhibit some degree of negative synergy close to the slot. The trend in increasing synergy with increasing gas injection rate from L to M and H is observed.

Figure 10 presents combined injection data for injection of 2000 w.p.p.m. polymer solution. The synergy traces for nearly all conditions, with the possible exception of the low/$5Q_S$ gas/polymer combination at 16 m s^{-1}, show no signs of peaking. We interpret this as indicating that the initial diffusion zone has been extended past the downstream drag balance toward the tail end of the plate. The synergy levels are roughly zero near the slot for all conditions. This indicates that the multiplicative condition is being realized at that location.

A comparison of the polymer-only data in figure 5 to the combined injection data in figures 8–10 shows that the synergistic benefit begins at conditions corresponding to the end of the extended initial diffusion zone with only polymer injection,

https://doi.org/10.1017/S0022112006009487 Published online by Cambridge University Press

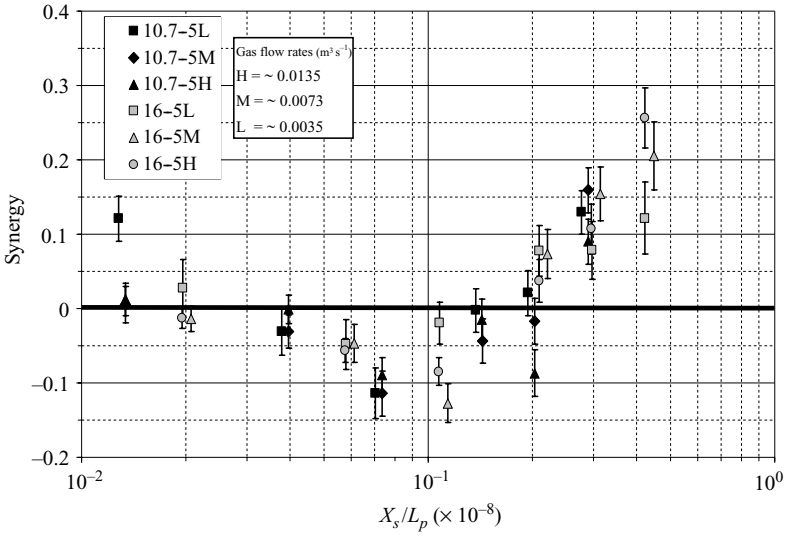


FIGURE 10. Synergy levels for air over 2000 p.p.m. UCARFLOC 309.

$X_S/L_p \times 10^{-8} \sim 0.1$ to 0.2 ($5 \leqslant K \times 10^8 \leqslant \sim 7$). At the X_S/L_p values where the polymer-only drag reductions begin to decrease from the peak levels, the combined injection results begin to exceed multiplicative behaviour. With combined injection, the drag reductions on figure 5 are sustained at the highest levels observed with polymer injection alone to X_S/L_p values that are 2 to over 4 times larger than with polymer alone. Synergy is maintained through the transition zone once drag reductions begin to decay with increasing X_S/L_p. The peak in synergy at $X_S/L_p \times 10^{-8} \sim 0.3$ to 0.5 ($K \times 10^8 \sim 2.5$ at $X_S/L_p = 0.4$) in figures 8 and 9, is interpreted as the end of the combined injection initial diffusion zone.

Increasing the near-wall concentration of the polymer at locations downstream of the polymer only initial-diffusion zone should result in increased drag reduction. This requires only that polymer-induced drag reduction is not near some maximum asymptotic limit. While detailed polymer wall concentration measurements were not conducted during this test, preliminary polymer wall concentration measurements using a florescence technique to estimate the polymer concentration at the surface under the bubble cloud have been performed using a fibre optic probe similar to that described in Fontaine, Petrie & DeVilbiss (2005). These preliminary measurements, conducted in another facility described by Fontaine *et al.* (2005), support the hypothesis that polymer wall concentrations are increased at downstream locations with combined injection. These results indicate that the addition of gas injection produces an increase in drag reduction from two sources: the independent addition of the microbubble drag reduction (which decreases rapidly with X); and increased polymer concentrations near the wall owing to the influence of the micro-bubble injection on the polymer diffusion.

The potential for a substantial increase in drag-reduction persistence with combined injection is the most compelling reason to consider combined injection. Persistence was estimated by comparing the distance over which a given level of integrated drag reduction can be achieved with polymer, gas or combined injection. To do this, a polynomial curve was fitted to the drag-reduction data as a function of X_S/L_p for polymer and combined injection and X_S/L_m for gas injection. These curve fits to the

https://doi.org/10.1017/S0022112006009487 Published online by Cambridge University Press

Polymer concentration w.p.p.m.	Polymer Q_s	Gas flow rate	U_e (m s^{-1})	Polymer injection		Gas injection		Combined injection		
				X_S/L_p	X_S (m)	X_S/L_m	X_S (m)	X_S/L_p	X_S (m)	X_S ratio
500	10	M	16	0.10	0.23	620	0.53	0.97	2.19	9.7
1000	5	M	16	0.27	0.62	620	0.53	1.00	2.28	3.7
2000	5	M	16	0.28	1.23	620	0.53	0.95	4.16	3.4
500	5	H	16	0.10	0.23	817	1.18	1.38	3.12	13.8
1000	5	H	16	0.27	0.62	817	1.18	1.30	2.96	4.8
2000	5	H	16	0.31	1.36	817	1.18	NA	NA	NA

NA: not available

TABLE 2. Comparison of $\sim 48\,\%$ total drag reduction for polymer, gas and combined injection.

data were then integrated to determine the average drag reduction as a function of X_S/L_p for polymer or combined injection and as a function of X_S/L_m for gas only injection using:

$$DR_{total} = L_p/X_s \int_0^{Xs/Lp} DR\, \mathrm{d}(X_s/L_p)$$

for polymer and combined injection, and

$$DR_{total} = L_m/X_s \int_0^{Xs/Lm} DR\, \mathrm{d}(X_s/L_m)$$

for gas injection. An estimate of the increased persistence for a specified integrated drag-reduction level was obtained by comparing the value of X_S/L_p or X_S/L_m that yields the specified integrated drag reduction. At a specified drag-reduction level, an increase in X_S/L_p with combined injection translates into the same increase in X (or persistence) for constant polymer Q_pC_i, gas injection and free-stream speed, assuming the scaling used is valid for the range of variables involved.

A comparison of estimated X_S/L_p and X_S/L_m corresponding to an integrated drag reduction of 48 % is provided in table 2 for gas, polymer and combined injection cases. An integrated drag reduction of 48 % was chosen as this is the maximum drag reduction for the polymer injection case of 2000 w.p.p.m. at $5Q_s$ injection, and approximates the average drag reduction for initial zone behaviour in most polymer-injection cases. The X_S/L_p and X_S/L_m columns also contain the estimated streamwise position (X_S) calculated from those X_S/L_p and X_S/L_m values using the defined velocity and injection parameters in table 2. The results indicate that significant increases in persistence can be obtained by combining the two systems, or conversely, higher levels of total drag reduction can be obtained for a specified axial length. For example, the distance from the slot, X_S, at which 48 % integrated drag reduction can be achieved with 500 w.p.p.m. UCARFLOC 309 injection alone is 0.23 m. Combining this polymer injection with a gas injection at the medium gas rate increases the estimated distance for 48 % integrated drag reduction to $X_S = 2.2$ m, a 9.7 times increase, as indicated in the X_S ratio column, $X_{Scombined}/X_{Spolymer}$. In addition, higher total drag reduction can be obtained with lower polymer consumption values (Q_pC_i) for combined injection compared to what is achieved with higher polymer Q_pC_i values for polymer injection alone.

https://doi.org/10.1017/S0022112006009487 Published online by Cambridge University Press

The decrease in X_S ratio with increasing polymer injection concentration also supports the premise that the synergistic benefit of combined injection has an impact on the length of the injected polymer solution initial diffusion zone. The short persistence length of the gas injection (see figure 4*a*) suggests that the effect of increasing polymer wall concentration by the gas layer may be limited to the persistence region of the gas. Increasing the length of the polymer only initial diffusion zone by increasing polymer concentration or polymer Q_pC_i may then reduce the overall impact of the gas layer if the polymer initial diffusion zone extends beyond the gas persistence zone. Furthermore, increasing the wall concentration of the high polymer injection concentration may extend the high polymer viscosity effects further downstream. Thus, we see a large relative increase in the X_S ratio values in the 500 w.p.p.m. polymer injection cases with gas injection when compared to the 2000 w.p.p.m. injection condition.

Increasing the gas injection rate from medium to high (a doubling of flow rate) increases the synergistic effect, as indicated in table 2. The increased persistence from combined injection may be related to the increased persistence with gas injection. The large X_S values (beyond the last measurement location) for combined injection are determined by assuming the combined injection follows the log–linear transition zone behaviour in DR *vs.* X_S/L_p for $X_S/L_p \times 10^{-8} > 0.5$. The polymer only injection of 2000 w.p.p.m. UCARFLOC 309 at $5Q_s$ and $16\,\mathrm{m\,s^{-1}}$ exhibits initial diffusion zone behaviour at approximately $X_S = 1.0\,\mathrm{m}$. The combined 2000 w.p.p.m. injection at $5Q_s$ with high gas injection extends the polymer initial diffusion zone to at least the last measurement location so that no transition zone behaviour is observed. The persistence length will be well beyond the end of the test plate. As a result, we have indicated this by the 'NA' entry in table 2.

Since Petrie *et al.* (1996) showed that polymer injection scales with X_S/L_p, a conservative estimate of the total integrated drag reduction and full persistence length can be obtained by extrapolating the transition zone region of the DR *vs.* X_S/L_p curve out to the point at which drag reduction is lost. Performing this exercise for the 2000 w.p.p.m. injection at $5Q_s$ yields a persistence length of 4.9 m with a total integrated drag reduction of $\sim 25\,\%$. The combined injection results for this polymer case with high gas injection, indicate a significant increase in persistence over the polymer only result since the initial zone appears to be extended to the end of the plate. It is likely that the increased persistence by combined high gas injection with the 2000 w.p.p.m. polymer injection at $5Q_s$ would be greater than 10 m based, for an average drag reduction of 25 %, on the X_S ratio results in table 2.

This increased effectiveness implies that combined injection will in some ways reduce drag-reduction-system requirements. Polymer expenditure can be reduced and persistence can be extended beyond what is achieved with polymer alone.

4. Conclusions

Injection of gas upstream of polymer injection produces increased levels of drag reduction with increased persistence. The increased level of drag reduction can be significantly higher than the multiplicative result expected for combined independent processes. The increased level of drag reduction and persistence is more than can be achieved by microbubble or polymer alone and implies that significant levels of total drag reduction can be obtained at more moderate expenditure rates of both polymer and micro-bubbles when combined. The combination of gas with polymer injection eliminates the increased drag penalty associated with high-concentration high-viscosity polymer solutions near the injector.

https://doi.org/10.1017/S0022112006009487 Published online by Cambridge University Press

Although polymer wall concentration measurements were not conducted during this study, the characteristics of the synergistic increase in drag reduction with dual injection of microbubbles upstream of the polymer are most probably a result of a reduction in the rate of diffusion of the polymer away from the wall. We speculate that this decreased diffusion rate serves to increase the streamwise extent of the polymer initial diffusion zone to produce larger drag reduction over greater distances downstream of the injection slot. An ongoing study has confirmed that local polymer wall concentrations can be increased substantially with gas injection.

Synergy is not observed where the polymer drag reduction is near a maximum, referred to here as the polymer-only initial diffusion zone. The polymer-only initial diffusion zone is the region of near-maximum drag reduction (Virk, Mickley & Smith 1970; Petrie *et al.* 1996*b*), due to the high near-wall polymer concentration. Thus, no significant increase in drag reduction due to increased near-wall polymer concentration by the microbubble injection can occur in this zone. Therefore, a synergistic effect is not observed at conditions corresponding to a polymer-only initial diffusion zone. While gas injection clearly offsets the negative effects of the high viscosity of the polymer near the slot, the negative synergy levels imply that the viscous drag penalty with high polymer concentrations may act to offset some of the multiplicative gains expected with combined injection in the initial diffusion zone.

Numerous studies have shown that drag reduction can be obtained by injection of different viscoelastic materials providing the materials exhibit certain characteristic rheological and molecular properties. Surfactant solutions and a variety of polymers (gums, polyacrylamides, PEOs, etc.) have been shown to be effective drag reducers. Although characteristics of the drag reduction mechanism (amount of drag reduction, persistence, resistance to degradation) and ease of use varies with the viscoelastic materials used, the fundamental mechanism for drag reduction is strongly dependent on the material concentration at the wall and the diffusion rate of this material away from the near-wall region. We believe that the microbubble-induced drag-reducing mechanism would still act independently of a viscoelastic-material-based drag-reduction mechanism regardless of the viscoelastic material used, provided the material did not exhibit characteristics that would adversely alter the bubble cloud behaviour, such as causing significant bubble coalescence. Furthermore, the effect of reduced polymer diffusion by the bubbles (bubble screening, reduced turbulent diffusion or de-coupling between inner and outer turbulent diffusion) would still occur with combined injection. Thus, the observed synergistic effect should occur with combined injection of microbubbles and a variety of viscoelastic drag-reducing materials, although, the overall characteristics of the synergistic process (magnitude and persistence) may vary with different drag-reducing viscoelastic materials used.

This work was supported in part by the Office of Naval Research (ONR) N00014-04-1-0753 with Dr Pat Purtell as technical monitor, and in part by The Applied Research Laboratory/Penn State University through internal R&D Funds.

REFERENCES

Bogdevich, V. G. & Evseev, A. R. 1976 Effect of gas saturation on wall turbulence. *Investigations of Boundary Layer Control*, Thermophysics Institute, Novosibirsk (in Russian).

Bogdevich, V. G. & Malyuga, A. G. 1976 The distribution of skin friction in a turbulent boundary layer. *Investigations of Boundary Layer Control*, Thermophysics Institute, Novosibirsk (in Russian).

https://doi.org/10.1017/S0022112006009487 Published online by Cambridge University Press

Brungart, T. A., Harbison, W., Petrie, H. L. & Merkle, C. L. 1991 A fluorescence technique for measurement of slot-injected fluid concentration profiles in a turbulent boundary layer. *Exps. Fluids* **11**, 9–16.

Coleman, H. G. & Steele, W. G. 1999 *Experimentation and Uncertainty Analysis for Engineers*. John Wiley.

Deutsch, S., Moeny, M. J., Fontaine, A. A. & Petrie, H. L. 2004 Microbubble drag reduction in rough walled turbulent boundary layers with comparison against polymer drag reduction. *Exps. Fluids* **37,** 731–744.

Deutsch, S. & Zierke, W. C. 1986 The measurement of boundary layers on a compressor blade in a cascade at high positive incidence angle. *NASA Contractor Rep.* 179492.

Fontaine, A. A. & Deutsch, S. 1992 The influence of the type of gas on the reduction of skin friction drag by microbubble injection. *Exps. Fluids* **13**, 128–136.

Fontaine, A. A., Deutsch, S., Brungart, T. A., Petrie, H. L. & Fenstermacker, M. 1999 Drag reduction by coupled systems: microbubble injection with homogeneous polymer and surfactant solutions. *Exps. Fluids* **26**, 397–403.

Fontaine, A. A., Petrie, H. L. & Brungart, T. A. 1992 Velocity profile statistics in a turbulent boundary layer with slot injected polymer. *J. Fluid Mech.* **238**, 435–466.

Fontaine, A. A., Petrie, H. L. & DeVilbiss, D. 2005 Void fraction and velocity probe for microbubble flow studies. *Second Intl Symp. on Seawater Drag Reduction*, sponsored by ONR and ASERC, Busan, Korea, pp. 391–404.

Housiadas, K. & Beris, A. 2003 Polymer induced drag reduction: effects of variations in elasticity and inertia in turbulent visco-elastic channel flow. *Phys. Fluids* **15**, 2369–2384.

Madavan, N. K., Deutsch, S. & Merkle, C. L. 1985 Measurements of local skin friction in a microbubble modified turbulent boundary layer. *J. Fluid Mech.* **156**, 237–256.

Malyuga, A., Mikuta, V. & Nenashev, A. 1989 Local drag reduction at flow of polymer solutions aerated by air bubbles. In *Proc. of the 6th National Congress of Theoretical and Applied Mathematics, 25–30 Sept. 1989, Varna, Bulgaria*, pp. 74-1–74-6.

Merkle, C. L. & Deutsch, S. 1989 Microbubble drag reduction. *Frontiers in Experimental Fluid Mechanics*, (ed. M. Gad el Hak), vol. 46, pp. 291–335. Springer.

Migirenko, G. S. & Evseev, A. R. 1974 Turbulent boundary layer with gas saturation. In *Problems of Thermophysics and Physical Hydrodynamics*, Novosibirsk, Nauka (in Russian).

Pal, S., Deutsch, S. & Merkle, C. L. 1989 A comparison of shear stress fluctuation statistics between microbubble modified and polymer modified turbulent boundary layers. *Phys. Fluids* A **1**, 1360–1362.

Petrie, H. L., Deutsch, S., Brungart, T. A. & Fontaine, A. A. 2003 Polymer drag reduction with surface roughness in flat-plate turbulent boundary layer flow. *Exps. Fluids* **35**, 8–23.

Petrie, H. L., Deutsch, S., Brungart, T. A. & Fontaine, A. A. 2004 Polymer drag reduction with surface roughness in flat-plate turbulent boundary layer flow (Errata). *Exps. Fluids* **36**, 663.

Petrie, H. L., Fontaine, A. A. & Brungart, T. A. 1996*a* Drag reduction on a flat plate at high Reynolds number, with slot-injected polymer solutions. In *Proc. ASME Fluids Engng Division Summer Meeting, ASME FED, San Diego, California, July 1996*, **237**, 3–9.

Petrie, H. L., Fontaine, A. A. & Brungart, T. A. 1996*b* Comparison of turbulent boundary layer modifications with slot injected and homogeneous drag reducing polymer solutions. In *Proc. ASME Fluids Engng Division Summer Meeting, ASME FED, San Diego, California, July 1996*, **237**, 201–210.

Petrie, H. L., Fontaine, A. A., Brungart, T. A. & Sommer, S. 1990 Large flat plate turbulent boundary layer evaluation. *ARL TM 89–207*.

Petrie, H. L., Fontaine, A. A., Moeny, M. J. & Deutsch, S. 2005 Experimental study of slot injected polymer drag reduction. *Second Intl Symp. on Seawater Drag Reduction*, sponsored by ONR and ASERC, Busan, Korea, pp. 605–619.

Philips, R., Castano, J. & Stace, J. 1998 Combined polymer and microbubble drag reduction. *Proc. of the Intl Symp. Seawater Drag Reduction, 22–23 July 1998, Newport RI*, pp. 335–340.

Poreh, M. & Cermak, J. E. 1964 Study of diffusion from a line source in a turbulent boundary layer. *Intl J. Heat Mass Transfer* **7**, 1083–1095.

Poreh, M. & Hsu, K. 1972 Diffusion of drag reducing polymer into a turbulent boundary layer. *J. Hydronaut.* **61**, 27–33.

https://doi.org/10.1017/S0022112006009487 Published online by Cambridge University Press

Smith, R. & Tiederman, W. G. 1990 Investigation into the mechanism of polymer thread drag reduction. *Rep*. PME-FM-90-1, Purdue University, School of Mechanical Engineering, West Lafayette, IN.

Tiederman, W. G., Luchik, T. S. & Bogard, D. G. 1985 Wall layer structure and drag reduction. *J. Fluid Mech*. **156**, 419–437.

Vdovin, A. V. & Smol'yakov, A. V. 1978 Diffusion of polymer solutions in a turbulent boundary layer. *Zh. Prikl. Mekh. Tekh. Fiz*. **2**, 66–73 (transl. in UDC 532.526, 196–201, Plenum).

Vdovin, A. V. & Smol'yakov, A. V. 1981 Turbulent diffusion of polymers in a turbulent boundary layer. *Zh. Prikl. Mekh. Tekh. Fiz*. **4**, 98–104 (transl. in UDC 532.526 (1982), 526–531, Plenum).

Virk, P. S., Mickley, H. S. & Smith, K. A. 1970 The ultimate asymptote and mean flow structure in Tom's phenomena. *Trans. ASME* E: *J. Appl. Mech*. **37**, 488–493.

White, F. M. 1974 *Viscous Fluid Flow*. McGraw-Hill.

Wu, J. & Tulin, M. P. 1972 Drag reduction by ejecting additive solutions into pure water boundary layer. Trans. *ASME* D: *J. Basic Engng* **94**, 749–756.

https://doi.org/10.1017/S0022112006009487 Published online by Cambridge University Press